Pneumatic pulse-width modulated pressure control via trajectory optimized fast-switching electromagnetic valves

authored by **T. Glück, W. Kemmetmüller, A. Pfeffer, and A. Kugi**

and published in *Proceedings of the 13th Mechatronics Forum, International Conference.*

Cite this article as:

T. Glück, W. Kemmetmüller, A. Pfeffer, and A. Kugi, "Pneumatic pulse-width modulated pressure control via trajectory optimized fast-switching electromagnetic valves", in *Proceedings of the 13th Mechatronics Forum, International Conference*, vol. 3/3, Linz, Austria, Sep. 2012, pp. 692–699

BibTex entry:

```
@InProceedings{GlueckME2012,
  Title = {Pneumatic pulse-width modulated pressure control via trajectory optimized fast-switching
      electromagnetic valves},
  Author = {T. Glück and W. Kemmetmüller and A. Pfeffer and A. Kugi},
  Booktitle = {Proceedings of the 13th Mechatronics Forum, International Conference},
  Year = {2012},
  Address = {Linz, Austria},
  Month = {Sept. 17-19},
  Pages = {692-699},
  Volume = {3/3},
  Url = {http://www.trauner.at/buchdetail.aspx?artnr=20193031}
}
```

Link to original paper:

Read more ACIN papers or get this document:

Contact:

Automation and Control Institute (ACIN)
Vienna University of Technology
Gusshausstrasse 27-29/E376
1040 Vienna, Austria

Internet: www.acin.tuwien.ac.at
E-mail: office@acin.tuwien.ac.at
Phone: +43 1 58801 37601
Fax: +43 1 58801 37699

Pneumatic Pulse-Width Modulated Pressure Control via Trajectory Optimized Fast-Switching Electromagnetic Valves

T. Glück, W. Kemmetmüller, A. Pfeffer, A. Kugi
Automation and Control Institute
Vienna University of Technology
Gusshausstrasse 27–29
1040 Vienna, Austria
Email: glueck@acin.tuwien.ac.at
kemmetmueller@acin.tuwien.ac.at
pfeffer@acin.tuwien.ac.at
kugi@acin.tuwien.ac.at

***Abstract*— The design of a pneumatic pulse-width modulated pressure control via trajectory optimized fast-switching electromagnetic valves is presented. Two fast-switching valves are used in a half bridge configuration for pressure control in a pneumatic volume. The valves are operated using a feedforward control, which guarantees soft landing and time optimality. The control performance and achievable noise reduction of the pulse-width modulated pressure control in combination with the optimized switching strategy is demonstrated by measurement results on an experimental test bench.**

I. Introduction

In many industrial applications, there is a demand for pneumatic systems that are controlled by cheap and reliable switching actuators. In automation applications, for instance, pneumatic piston actuators are frequently controlled by means of pneumatic pulse-width modulation, see, e.g., [9], [12], [13], [14]. Here, four fast-switching valves, arranged in a pneumatic full bridge, replace the traditional directional control valve. In order to achieve a high pulse-width modulation frequency and likewise a high closed-loop bandwidth, short valve switching times are necessary. The high pulse-width modulation frequency, however, produces acoustic noise and causes mechanical wear of the valves. For this, so-called soft landing strategies were developed in recent years, cf. [5], [6].

In [8], the design of a feedforward controller that facilitates soft landing and time optimality of a fast-switching electromagnetic valve was presented. The feedforward controller was designed by point-to-point quasi-time-optimal control, which allows to incorporate input constraints in a systematic way. In this contribution, the feedforward control concept is applied to two fast-switching valves which are arranged in a pneumatic half bridge in order to control the pressure in a chamber by means of pulse-width modulation. For this, the mathematical model of the chamber is derived and the model parameters are identified by means of measurements. Furthermore, a nonlinear controller based on exact input-output linearization is designed.

At first, in Section II and III, the modeling of the switching valves and the design of the feedforward controller are briefly summarized. Subsequently in Section IV the chamber model is derived and in Section V the pulse-width modulated pressure control is designed. Measurement results on an experimental test bench, given in Section VI, validate the performance of the developed control strategy and demonstrate the resulting noise reduction.

II. Valve Model

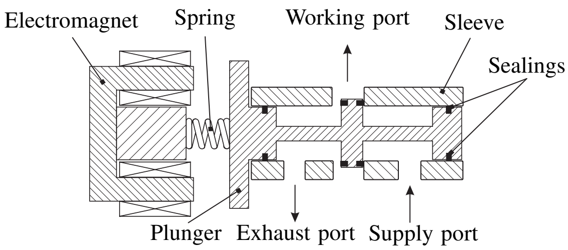

Fig. 1: Schematics of the $3/2$-fast-switching valve.

The mathematical model of the considered fast-switching valve, schematically depicted in Fig. 1, can be separated into three subsystems: the electromagnetic, the mechanical and the pneumatic subsystem. Since measurement results of the considered fast-switching valve confirm that the valve is pressure-balanced, the pressure forces acting on the plunger will be neglected. In addition, it is assumed that the flow force is small in comparison to the magnetic force. Since no internal feedback from the pneumatic dynamics to the electromechanical subsystem is considered, the optimal control

Post-print version of the article: T. Glück, W. Kemmetmüller, A. Pfeffer, and A. Kugi, “Pneumatic pulse-width modulated pressure control via trajectory optimized fast-switching electromagnetic valves”, in *Proceedings of the 13th Mechatronics Forum, International Conference*, vol. 3/3, Linz, Austria, Sep. 2012, pp. 692–699

problem can be formulated with the pneumatic subsystem being neglected.

A. Electromagnetic Subsystem

The equivalent magnetic circuit of the fast-switching valve is shown in Fig. 2a. It comprises the flux-dependent effective

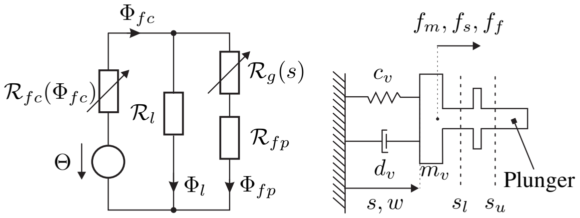

(a) Reluctance model. (b) Schematics.

Fig. 2: Reluctance model and schematics of the fast-switching valve.

core reluctance $\mathcal{R}_{fc}(\Phi_{fc})$, with core flux Φ_{fc}, the effective reluctance $\mathcal{R}_{fp}$ of the plunger, the effective reluctance $\mathcal{R}_g(s)$ of the air gap s between the core and the plunger, and the reluctance $\mathcal{R}_l$ which accounts for leakage fluxes. The reluctances are modeled in the form

$$\begin{aligned}\mathcal{R}_{fc}(\Phi_{fc}) &= \frac{l_{fc}}{\mu_0\mu_{fc}(\Phi_{fc})A_{fc}}, & \mathcal{R}_{fp} &= \frac{l_{fp}}{\mu_0\mu_{fp}A_{fp}}, \\ \mathcal{R}_l &= \frac{l_l}{\mu_0 A_l}, & \mathcal{R}_g(s) &= \frac{2s}{\mu_0 A_g}.\end{aligned} \tag{1}$$

Here, l_{fc}, l_{fp}, and l_l are the effective lengths of the core, the plunger, and the leakage flux lines, respectively. A_{fc}, A_{fp}, and A_l are the corresponding effective areas. The effective length of the air gap is equal to $2s$, since there are two air gaps between the core and the plunger, cf. Fig. 1. The corresponding area is denoted by A_g. Furthermore, μ_0 denotes the permeability of air and the relative permeability μ_{fp} of the plunger is assumed to be constant. Saturation of the core is phenomenologically modeled as

$$\mu_{fc}(\Phi_{fc}) = \left(k_1\left(\frac{|\Phi_{fc}|}{A_{fc}}\right)\exp\left(k_2\frac{|\Phi_{fc}|}{A_{fc}}\right) + k_3\right)^{-1}, \tag{2}$$

with the constant parameters k_j, $j = 1, 2, 3$. The equivalent reluctance $\mathcal{R}$ of the overall system reads as

$$\mathcal{R}(\Phi_{fc}, s) = \mathcal{R}_{fc}(\Phi_{fc}) + \frac{\mathcal{R}_l\left(\mathcal{R}_g(s) + \mathcal{R}_{fp}\right)}{\mathcal{R}_l + \mathcal{R}_g(s) + \mathcal{R}_{fp}}. \tag{3}$$

Using the magnetomotive force $\Theta = Ni$ of the coil, where i is the current and N is the number of turns, the flux Φ_{fc} through the coil is given in the form

$$\Phi_{fc} = \frac{\Theta}{\mathcal{R}}. \tag{4}$$

Based on the flux linkage $\psi = N\Phi_{fc}$ of the coil, Faraday's law yields

$$\frac{\mathrm{d}}{\mathrm{d}t}\psi = v - Ri, \quad \psi(0) = \psi_0 \tag{5}$$

with initial condition ψ_0, the electric resistance R and the applied voltage v. Moreover, the coil current i can be expressed in terms of the flux linkage and the air gap in the form

$$i = \frac{\mathcal{R}(\psi, s)}{N^2}\psi. \tag{6}$$

B. Mechanical Subsystem

Fig. 2b shows a schematic diagram of the forces acting on the plunger of the fast-switching valve. Here, s is the plunger position and $w = \dot{s}$ is the plunger velocity. The mass of the plunger is denoted by m_v, the stiffness of the load spring by c_v, and the viscous damping coefficient due to the friction of the housing and the sealing elements by d_v. The plunger is loaded by the magnetic force $f_m(\psi, s)$, the spring force $f_s(s)$ and the friction force $f_f(w)$. Based on the magnetic energy with (3) and (6), see, e.g., [7],

$$\begin{aligned}\mathcal{W}_m(\psi, s) &= \int_0^\psi i(\tilde{\psi}, s)\mathrm{d}\tilde{\psi} \\ &= \int_0^\psi \frac{\mathcal{R}_{fc}(\tilde{\psi}/N)}{N^2}\tilde{\psi}\mathrm{d}\tilde{\psi} \\ &\quad + \frac{1}{2N^2}\frac{\mathcal{R}_l\left(\mathcal{R}_g(s) + \mathcal{R}_{fp}\right)}{\mathcal{R}_l + \mathcal{R}_g(s) + \mathcal{R}_{fp}}\psi^2\end{aligned} \tag{7}$$

the magnetic force yields

$$\begin{aligned}f_m(\psi, s) &= -\left(\frac{\partial}{\partial s}\mathcal{W}_m\right)(\psi, s) \\ &= -\frac{1}{2N^2}\frac{\mathcal{R}_l^2}{\left(\mathcal{R}_l + \mathcal{R}_g(s) + \mathcal{R}_{fp}\right)^2}\left(\frac{\partial}{\partial s}\mathcal{R}_g\right)(s)\psi^2.\end{aligned} \tag{8}$$

The spring force is modeled as

$$f_s(s) = -c_v\left(s - l_{c0}\right) \tag{9}$$

with the preload force $c_v l_{c0}$. The friction force is assumed to be composed of Coulomb friction and viscous friction, i.e.

$$f_f(w) = -f_{fc}\,\mathrm{sign}(w) - d_v w, \tag{10}$$

where the Coulomb friction force is denoted by f_{fc} and the viscous damping coefficient by d_v. Henceforth, the signum-function in (10) is approximated by $\tanh\left(\frac{w}{w_c}\right) \approx \mathrm{sign}(w)$, with $w_c \ll 1$, providing a continuously differentiable friction force $f_f(w)$. The balance of momentum for the plunger and Faraday's law (5) with (6) and the reluctance model (3) results in the mathematical model

$$\frac{\mathrm{d}}{\mathrm{d}t}s = w, \qquad s(0) = s_0, \tag{11a}$$

$$\frac{\mathrm{d}}{\mathrm{d}t}w = \frac{1}{m_v}\left(f_m(\psi, s) + f_s(s) + f_f(w)\right), \quad w(0) = w_0, \tag{11b}$$

$$\frac{\mathrm{d}}{\mathrm{d}t}\psi = v - R\frac{\mathcal{R}(\psi, s)}{N^2}\psi, \qquad \psi(0) = \psi_0. \tag{11c}$$

III. Trajectory Optimization

The mathematical model (11) with the state vector $\boldsymbol{x} = \begin{bmatrix} s & w & \psi \end{bmatrix}^\mathsf{T}$ and with the constrained, affine input $u = v \in \mathcal{U} = \begin{bmatrix} u^-, u^+ \end{bmatrix}$ can be written in the form

$$\frac{\mathrm{d}}{\mathrm{d}t}\boldsymbol{x} = \boldsymbol{f}(\boldsymbol{x}) + \boldsymbol{b}u, \quad \boldsymbol{x}(0) = \boldsymbol{x}_0, \tag{12}$$

with the initial condition $\boldsymbol{x}_0 = \begin{bmatrix} s_0 & w_0 & \psi_0 \end{bmatrix}^\mathsf{T}$, the vector field $\boldsymbol{f}$ and the constant input vector $\boldsymbol{b}$. The control objective is to find an optimal control input that guarantees a minimal transition time t_f for a setpoint change

$$(u_0, \boldsymbol{x}_0) \rightarrow (u_f, \boldsymbol{x}_f), \tag{13}$$

with

$$\begin{aligned} \boldsymbol{x}(0) = \boldsymbol{x}_0, u(0) &= u_0 : \quad \boldsymbol{0} = \boldsymbol{f}(\boldsymbol{x}_0) + \boldsymbol{b}u_0, \\ \boldsymbol{x}(t_f) = \boldsymbol{x}_f, u(t_f) &= u_f : \quad \boldsymbol{0} = \boldsymbol{f}(\boldsymbol{x}_f) + \boldsymbol{b}u_f \end{aligned} \tag{14}$$

and the terminal condition $\boldsymbol{x}(t_f) = \boldsymbol{x}_f$. Therefore, the input-constrained point-to-point optimal control problem

$$\begin{aligned} &\min_{u\in\mathcal{U}} \; J(u) = \varphi(t_f) + \int_0^{t_f} l(u)\mathrm{d}t \\ &\text{s.t.} \quad \frac{\mathrm{d}}{\mathrm{d}t}\boldsymbol{x} = \boldsymbol{f}(\boldsymbol{x}) + \boldsymbol{b}u, \; \boldsymbol{x}(0) = \boldsymbol{x}_0, \; \boldsymbol{x}(t_f) = \boldsymbol{x}_f, \\ &\qquad u \in \mathcal{U} = \begin{bmatrix} u^-, u^+ \end{bmatrix} \end{aligned} \tag{15}$$

has to be solved. In the quasi-time-optimal case, the terminal cost

$$\varphi(t_f) = t_f \tag{16}$$

assures the time optimality and the Lagrange density

$$l(u) = \frac{1}{2}ru^2, \tag{17}$$

with $r > 0$, serves as a regularization term in order to avoid singular arcs. Introducing the Hamiltonian, see, e.g., [4],

$$\mathcal{H}(\boldsymbol{x}, u, \boldsymbol{\lambda}) = l(u) + \boldsymbol{\lambda}^\mathsf{T}\left(\boldsymbol{f}(\boldsymbol{x}) + \boldsymbol{b}u\right), \tag{18}$$

with the adjoint states $\boldsymbol{\lambda}$, and applying a time transformation $t = t_f^*\tau$ that maps the time interval $t \in (0, t_f^*)$ onto $\tau \in (0,1)$, the optimal control problem can be reformulated by means of Pontryagin's maximum principle, see, e.g., [3], in form of a two-point boundary value problem, i.e.

$$\frac{\mathrm{d}}{\mathrm{d}\tau}\begin{bmatrix} \boldsymbol{x}^* \\ \boldsymbol{\lambda}^* \end{bmatrix} = t_f^*\begin{bmatrix} \boldsymbol{f}(\boldsymbol{x}^*) \\ -\left(\frac{\partial}{\partial \boldsymbol{x}}\boldsymbol{f}\right)^\mathsf{T}(\boldsymbol{x}^*)\,\boldsymbol{\lambda}^* \end{bmatrix} + t_f^*\begin{bmatrix} \boldsymbol{b} \\ \boldsymbol{0} \end{bmatrix} u^* \tag{19a}$$

$$u^* = \arg\min_{u\in\mathcal{U}} \mathcal{H}(\boldsymbol{x}^*, u, \boldsymbol{\lambda}^*) \tag{19b}$$

with boundary conditions

$$\boldsymbol{x}^*(0) = \boldsymbol{x}_0 \quad \text{and} \quad \boldsymbol{x}^*(1) = \boldsymbol{x}_f \tag{19c}$$

and the transversality condition

$$\mathcal{H}(\boldsymbol{x}^*, u^*, \boldsymbol{\lambda}^*)|_{\tau=1} = -1 \tag{19d}$$

resulting from the free end time t_f^*. Here, the superscript * refers to optimal variables.

A. Solution of the Quasi-Time-Optimal Control Problem

Owing to the input affine system representation (12), the first-order necessary condition arising from the minimization problem (19b) reads in the unconstrained case as

$$\left(\frac{\partial}{\partial u}\mathcal{H}\right)(\boldsymbol{x}^*, u^0, \boldsymbol{\lambda}^*) = ru^0 + (\boldsymbol{\lambda}^*)^\mathsf{T}\boldsymbol{b} = 0 \tag{20}$$

and can be explicitly solved in the form

$$u^0 = -\frac{1}{r}(\boldsymbol{\lambda}^*)^\mathsf{T}\boldsymbol{b}. \tag{21}$$

In the constrained case it can be easily seen that the optimal control input takes the form

$$u^* = \xi(\boldsymbol{\lambda}^*) = \begin{cases} u^- & \text{for} \quad u^0 \leq u^- \\ u^0 & \text{for} \quad u^0 \in (u^-, u^+) \\ u^+ & \text{for} \quad u^0 \geq u^+ \end{cases}. \tag{22}$$

Note that in the present case $(\boldsymbol{\lambda}^*)^\mathsf{T}\boldsymbol{b} = \lambda_3^*$. Considering the limit case $r \rightarrow 0$ the optimal control input u^* switches between the limits u^- and u^+ whenever λ_3^* changes the sign. Then, the solution of the optimal control problem (15) is a bang-bang control.

In addition to (20), the second-order necessary optimality condition, the so-called Legendre-Clebsch condition

$$\left(\frac{\partial^2}{\partial u^2}\mathcal{H}\right)(\boldsymbol{x}^*, u^*, \boldsymbol{\lambda}^*) \geq 0, \tag{23}$$

is fulfilled, for $r > 0$.

B. Results of the Trajectory Optimization for Soft-Landing

For the opening and for the closing of the valve, respectively, the point-to-point transitions

$$\left(u_0 = v_u, \; \boldsymbol{x}_0 = \begin{bmatrix} s_u \\ 0 \\ \psi_u \end{bmatrix}\right) \rightarrow \left(u_f = v_l, \; \boldsymbol{x}_f = \begin{bmatrix} s_l \\ 0 \\ \psi_l \end{bmatrix}\right) \tag{24}$$

and

$$\left(u_0 = v_l, \; \boldsymbol{x}_0 = \begin{bmatrix} s_l \\ 0 \\ \psi_l \end{bmatrix}\right) \rightarrow \left(u_f = v_u, \; \boldsymbol{x}_f = \begin{bmatrix} s_u \\ 0 \\ \psi_u \end{bmatrix}\right) \tag{25}$$

have to be performed within the normalized transition time $\tau \in (0,1)$. Here, v_l, ψ_l denote the resulting setpoint voltage and flux linkage at the lower end stop s_l and v_u, ψ_u the setpoint voltage and flux linkage at the upper end stop s_u, cf. (14).

C. Numerical Results of the Quasi-Time-Optimal Control Problem

Numerical solutions of the two-point boundary value problem (19) with (21) and (22) can be obtained by utilizing the MATLAB function `bvp5c`, cf. [11]. The function `bvp5c` implements a finite difference method, in particular a collocation method, see [11], that controls a scaled residual

Post-print version of the article: T. Glück, W. Kemmetmüller, A. Pfeffer, and A. Kugi, "Pneumatic pulse-width modulated pressure control via trajectory optimized fast-switching electromagnetic valves", in *Proceedings of the 13th Mechatronics Forum, International Conference*, vol. 3/3, Linz, Austria, Sep. 2012, pp. 692–699

and the true error, and adapts the mesh grid. The solver may not find a solution if the initial guess does not adequately represent the behavior of the system, see, e.g., [11]. As the adequate initial guess is not easy to find, especially for the adjoint variables, there is a need for a systematic solution procedure. The two-point boundary value problem is therefore numerically solved in a sequential procedure that can be summarized as follows:

First, a uniform mesh of $M = 30$ grid points at the time steps $\tau_k = kT_k$, $k = 0, 1, \ldots, M$, $T_k = 1/M$ serve as initial guess for the trajectories $\boldsymbol{x}^*(\tau_k)$, $\boldsymbol{\lambda}^*(\tau_k)$. A linear interpolation is performed between the boundary conditions (19c) of the states $\boldsymbol{x}$ with the setpoint from (24) for the opening and (25) for the closing, and zero initial values of the adjoint states $\boldsymbol{\lambda}$ are assumed. Then, the problem is solved recurrently for a sequence of parameters $r = r_{\text{start}}, \ldots, r_{\text{end}}$, cf. (17), using the previously received solution as new initial guess.

Figures 3 and 4 show numerical results of the quasi-time-optimal point-to-point transition for the opening and for the closing scenario for decreasing parameters $r \in [10^{-1}, 10^{-2}, 10^{-3}, 10^{-6}]1/\text{V}^2$. Note that for all numerical solutions outside the vertical dashed lines the initial and final values are held constant for illustration purposes only.

The optimal state trajectories for opening the valve are given in Fig. 3a. Fig. 3c shows the corresponding optimal input voltage v^*, which converges for smaller parameters $r \to 0$ towards a bang-bang control. Fig. 4 shows analogous numerical results for the closing scenario of the valve. Note that in this case the solution of the optimal control problem is not purely bang-bang. Whenever λ_3^* vanishes, i.e. approximately for the time interval $\mathcal{I}_s = [\tau_1, \tau_2] \approx [0.3, 0.4]$, u^* vanishes as well. This happens if f_m^* vanishes, implying that only the spring force accelerates the plunger. Parameter studies have shown that this singular arc can be avoided with a smaller plunger mass m_v, a smaller damping coefficient d_v, a larger spring stiffness c_v or a larger preload force $c_v l_{c_0}$.

IV. Chamber and Pneumatic Valve Model

In the considered application, a half bridge comprising two fast-switching valves is used for pressure control in a chamber, see Fig. 5. The chamber can be described by two independent variables, the temperature ϑ and the pressure p, and the governing model equations may be derived from the conservation of mass and energy, see, e.g., [10]. Stipulating an isentropic process, the change of internal energy $\dot{U}$ is equal to the sum of the enthalpy flow $\dot{H} = \dot{m}_{\text{in}} h_{\text{in}} - \dot{m}_{\text{out}} h_{\text{out}}$ and the applied heat flow $\dot{Q} = A\beta(\vartheta_{\text{amb}} - \vartheta)$, that is

$$\frac{\mathrm{d}}{\mathrm{d}t} U = \dot{m}_{\text{in}} h_{\text{in}} - \dot{m}_{\text{out}} h_{\text{out}} + A\beta(\vartheta_{\text{amb}} - \vartheta), \tag{26}$$

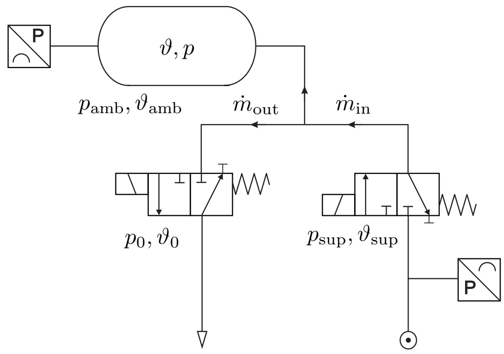

Fig. 5: Setup with pneumatic half bridge.

with mass flow $\dot{m}_j$, specific enthalpy h_j, $j \in \{\text{in}, \text{out}\}$, heat transfer coefficient β, chamber surface A and ambient air temperature ϑ_{amb}. Subsequently, it is assumed that the air obeys the ideal gas law $pV = R_s \vartheta m$, with mass m, pressure p, volume V and specific gas constant R_s. In addition, the caloric state equations for the ideal gas $\mathrm{d}u_j = c_v \mathrm{d}\vartheta_j$ and $\mathrm{d}h_j = c_p \mathrm{d}\vartheta_j$, with specific internal energy $u_j = U_j/m$, specific enthalpy $h_j = H_j/m$ and the constant, specific heat capacities c_v and c_p hold. With $R_s = c_p - c_v$ and the constant isentropic exponent $\kappa = c_p/c_v$, the temperature differential equation can be directly inferred form (26) using the mass balance (29)

$$\frac{\mathrm{d}}{\mathrm{d}t}\vartheta = \frac{(\kappa-1)\vartheta}{pV}\Big(\dot{m}_{\text{in}}\left(c_p\vartheta_{\text{in}} - c_v\vartheta\right) - \dot{m}_{\text{out}}\left(c_p - c_v\right)\vartheta + A\beta(\vartheta_{\text{amb}} - \vartheta)\Big), \tag{27}$$

with initial temperature $\vartheta(0) = \vartheta_0$. The change of the gas temperature at the inflow valve can be approximated according to an isentropic change

$$\vartheta_{\text{in}} = \vartheta_{\text{sup}} \left(\frac{p_{\text{sup}}}{p}\right)^{\frac{1-\kappa}{\kappa}}, \tag{28}$$

where the index sup refers to the supply variables. The consideration of the mass balance

$$\frac{\mathrm{d}}{\mathrm{d}t} m = \frac{\mathrm{d}}{\mathrm{d}t}(\rho V) = \dot{m}_{\text{in}} - \dot{m}_{\text{out}} \tag{29}$$

with ρ in (29) $\rho = p/(R_s\vartheta)$ according to the ideal gas law in combination with (27) gives rise to the pressure differential equation

$$\frac{\mathrm{d}}{\mathrm{d}t} p = \frac{\kappa R_s}{V}\left(\dot{m}_{\text{in}}\vartheta_{\text{in}} - \dot{m}_{\text{out}}\vartheta\right) + \frac{\kappa - 1}{V} A\beta(\vartheta_{\text{amb}} - \vartheta), \tag{30}$$

with initial pressure $p(0) = p_0$. The adiabatic lossless flow through a throttle valve, according to ISO [2], is given by

$$\dot{m}_j = C_j(s_j) p_j \rho_0 \sqrt{\frac{\vartheta_0}{\vartheta_j}} \Psi(\Pi_j), \quad j \in \{\text{in}, \text{out}\}, \tag{31}$$

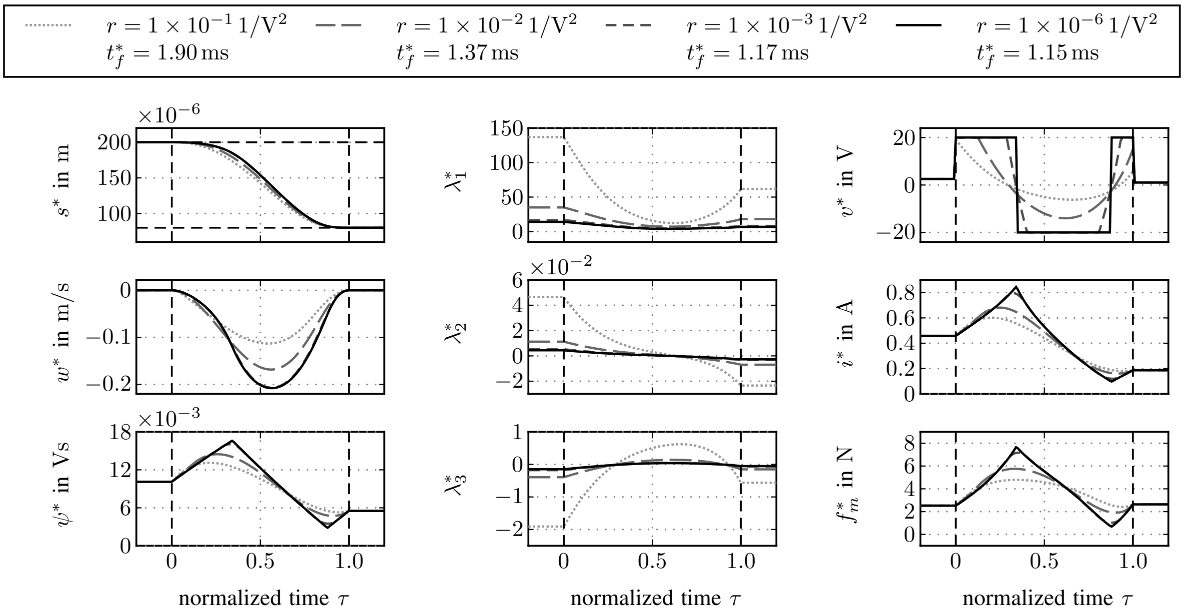

(a) Optimal state trajectories.

(b) Optimal adjoint state trajectories.

(c) Optimal voltage v^*, current i^*, magnetic force f_m^*.

Fig. 3: Numerical results of the quasi-time-optimal control problem for the opening motion ($s_u \rightarrow s_l$).

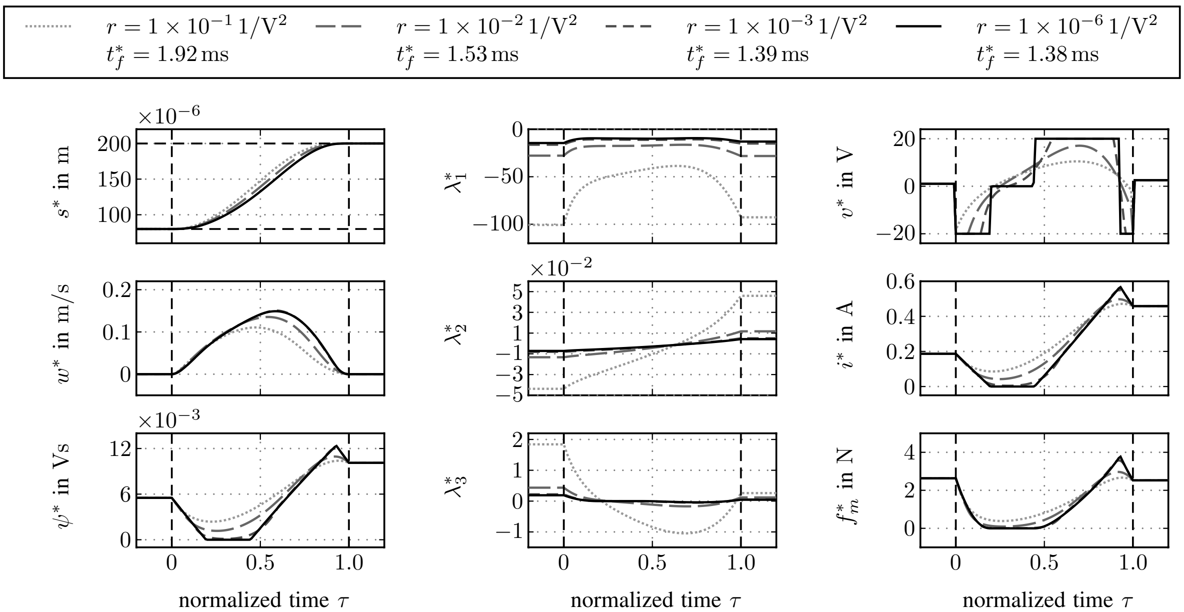

(a) Optimal state trajectories.

(b) Optimal adjoint state trajectories.

(c) Optimal voltage v^*, current i^*, magnetic force f_m^*.

Fig. 4: Numerical results of the quasi-time-optimal control problem for the closing motion ($s_l \rightarrow s_u$).

Post-print version of the article: T. Glück, W. Kemmetmüller, A. Pfeffer, and A. Kugi, "Pneumatic pulse-width modulated pressure control via trajectory optimized fast-switching electromagnetic valves", in *Proceedings of the 13th Mechatronics Forum, International Conference*, vol. 3/3, Linz, Austria, Sep. 2012, pp. 692–699
The content of this post-print version is identical to the published paper but without the publisher's final layout or copy editing.

with technical density $\rho_0 = 1.1845\,\mathrm{kg/m^3}$ and technical temperature $\vartheta_0 = 293.15\,\mathrm{K}$. The position-dependent pneumatic conductances C_j are assumed to be affine in the valve position s_j and read as $C_j(s_j) = \gamma(s_u - s_j)$ with constant $\gamma > 0$ and upper limit s_u for $j \in \{\mathrm{in}, \mathrm{out}\}$. The flow-through function $\Psi(\Pi_j)$ in (31) is described by [2]

$$\Psi(\Pi_j) = \begin{cases} \sqrt{1 - \left(\frac{\Pi_j - \Pi_c}{1 - \Pi_c}\right)^2} & \text{for} \quad \Pi_j > \Pi_c \\ 1 & \text{for} \quad \Pi_j \leq \Pi_c \end{cases} \tag{32}$$

with pressure ratios $\Pi_{\mathrm{in}} = p_{\mathrm{sup}}/p$, $\Pi_{\mathrm{out}} = p/p_{\mathrm{amb}}$ and respective constant, critical pressure ratios $\Pi_c > 0$.

V. Pneumatic Pulse-Width Modulated Pressure Control

The usage of a pulse-width modulated valve opening area and likewise conductance C results in a pulse-width modulation of the mass flow $\dot{m}$, which allows to control the chamber pressure. Since the valve dynamics is reasonably

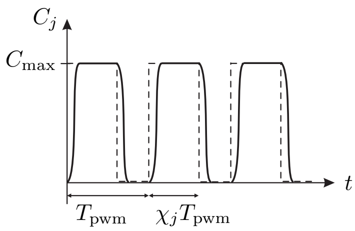

Fig. 6: Pulse-width modulated conductance.

fast compared to the temperature and pressure dynamics, the instantaneous switching of the valves may be assumed in the following. Using a suitable control strategy for the two valves of the half bridge as has been discussed in Section IV, either the maximum conductance $C_{\max}$ or the minimum conductance $C_{\min} = 0$ of the individual valves $j \in \{\mathrm{in}, \mathrm{out}\}$ can be prescribed. The pulse-width modulated conductances $C_j(t)$ for $t = kT_{\mathrm{pwm}}$ with $k \in \mathbb{Z}$ read as

$$C_j(t) = \begin{cases} C_{\max} & \text{for} \quad kT_{\mathrm{pwm}} < t \leq (k + \chi_j)T_{\mathrm{pwm}} \\ 0 & \text{for} \quad (k + \chi_j)T_{\mathrm{pwm}} < t \leq (k+1)T_{\mathrm{pwm}} \end{cases}, \tag{33}$$

where $0 \leq \chi_j \leq 1$ are the duty ratios and T_{pwm} is the fixed modulation period, cf. Fig. 6. Obviously, the average values

$$\bar{C}_j = \frac{1}{T_{\mathrm{pwm}}} \int_{(k-1)T_{\mathrm{pwm}}}^{kT_{\mathrm{pwm}}} C_j(t)\,\mathrm{d}t = C_{\max}\chi_j \tag{34}$$

of the conductances C_j can be directly determined by means of the pulse ratios χ_j. However, the value of the duty ratios χ_j can be solely set at the beginning of each modulation period. Hence, only the mean value $\bar{p}$ of the pressure and the mean value of the mass flow $\bar{\dot{m}}$ can be controlled via the duty ratios χ_j. For the controller design it is assumed that the overall gas temperature is constant, i.e. $\vartheta = \vartheta_{\mathrm{in}} = \vartheta_0 = \vartheta_{\mathrm{sup}}$. Then, the dynamics of the mean value $\bar{p}$ of the pressure

$$\bar{p} = \frac{1}{T_{\mathrm{pwm}}} \int_{t - T_{\mathrm{pwm}}}^{t} p(\tau)\,\mathrm{d}\tau \tag{35}$$

can be directly deduced from (30) in the form

$$\frac{\mathrm{d}}{\mathrm{d}t}\bar{p} = \frac{\kappa R_s}{V}\vartheta_0\left(\bar{\dot{m}}_{\mathrm{in}} - \bar{\dot{m}}_{\mathrm{out}}\right), \tag{36}$$

with the mass flow mean values

$$\bar{\dot{m}}_j = \frac{1}{T_{\mathrm{pwm}}} \int_{t - T_{\mathrm{pwm}}}^{t} \dot{m}_j(\tau)\,\mathrm{d}\tau \tag{37}$$

and $\dot{m}_j$ in accordance to (31). The interconnection of the fast-switching valves with $\dot{m}_{\mathrm{in}} \geq 0$ and $\dot{m}_{\mathrm{out}} \geq 0$ suggests to introduce the virtual control input

$$\alpha = \xi\bar{\dot{m}} = \xi\left(\bar{\dot{m}}_{\mathrm{in}} - \bar{\dot{m}}_{\mathrm{out}}\right), \tag{38}$$

whit the abbreviation $\xi = \kappa R_s \vartheta_0 / V$. Thus, the control law

$$\alpha = \dot{\bar{p}}_d - \eta_1 e_{\bar{p}} - \eta_0 e_{\bar{p},I}, \tag{39}$$

with the pressure error $e_{\bar{p}} = \bar{p} - \bar{p}_d$ and a sufficiently smooth desired trajectory $\bar{p}_d$ of the mean value of the pressure renders the linear error dynamics

$$\ddot{e}_{\bar{p}} + \eta_1 \dot{e}_{\bar{p}} + \eta_0 e_{\bar{p}} = 0. \tag{40}$$

The dynamics can be arbitrarily assigned by means of the positive control parameters $\eta_1, \eta_0 > 0$. The conditional integration

$$e_{\bar{p},I} = \int_0^t e_{\bar{p},c}\,\mathrm{d}\tau \quad \text{with}$$
$$e_{\bar{p},c} = \begin{cases} 0 & \text{if} \quad (\chi \geq \chi_{\max}) \wedge (e_{\bar{p}} > 0) \\ 0 & \text{if} \quad (\chi \leq \chi_{\min}) \wedge (e_{\bar{p}} < 0) \\ e_{\bar{p}} & \text{else} \end{cases} \tag{41}$$

is introduced in order to prevent control windup induced by the limits $\chi_{\min} \leq \chi \leq \chi_{\max}$. According to (38), the mass flows read as

$$\bar{\dot{m}}_{\mathrm{in}} = \begin{cases} \frac{\alpha}{\xi} & \text{for} \quad \alpha > 0 \\ 0 & \text{for} \quad \alpha \leq 0 \end{cases}, \quad \bar{\dot{m}}_{\mathrm{out}} = \begin{cases} 0 & \text{for} \quad \alpha \geq 0 \\ \frac{\alpha}{\xi} & \text{for} \quad \alpha < 0 \end{cases}. \tag{42}$$

Since the supply and ambient pressure, p_{sup} and p_{amb}, are assumed to be constant, the mass flow mean value (37) may be written in the form

$$\bar{\dot{m}}_j = \frac{\rho_0}{T_{\mathrm{pwm}}} \int_{t - T_{\mathrm{pwm}}}^{t} C_j(s_j)\Gamma(p_j)\,\mathrm{d}\tau, \tag{43}$$

with the pressure-dependent term $\Gamma(p_j) = p_j\Psi(\Pi_j)$. Moreover, for small pressure variations Δp_j from the mean values $\bar{p}_j$ the following approximation

$$\Gamma(p_j) \approx \Gamma(\bar{p}_j) + \mathcal{O}(|\Delta p_j|), \tag{44}$$

Post-print version of the article: T. Glück, W. Kemmetmüller, A. Pfeffer, and A. Kugi, "Pneumatic pulse-width modulated pressure control via trajectory optimized fast-switching electromagnetic valves", in *Proceedings of the 13th Mechatronics Forum, International Conference*, vol. 3/3, Linz, Austria, Sep. 2012, pp. 692–699
The content of this post-print version is identical to the published paper but without the publisher's final layout or copy editing.

with the Landau-symbol $\mathcal{O}(\cdot)$, see, e.g., [15], is utilized. The combination of the this approximation with (34) and (43) finally yields the duty ratios

$$\chi_j = \frac{1}{\rho_0 \Gamma(\bar{p}_j) C_{\max}} \bar{\dot{m}}_j, \quad j \in \{\text{in}, \text{out}\}, \tag{45}$$

which can be directly translated into closing times of the respective valves.

VI. Implementation

After the successful testing of the pulse-width modulated control strategy in several simulations, it was implemented on a test bench, see Figures 5 and 7 for the setup. The test bench

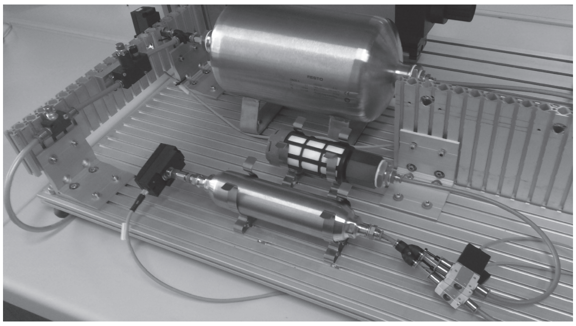

Fig. 7: Photograph of the test bench.

consists of two fast-switching valves and a chamber of volume $V = 0.4\,\mathrm{l}$. The real-time system DSPACE 1005 was used for data processing with a sampling time of $T_s = 10\,\mu\mathrm{s}$ and a modulation period of $T_{\mathrm{pwm}} = 10\,\mathrm{ms}$. Two pressure sensors measure the chamber and the supply pressure, p and p_{sup}, respectively. The latter was controlled by means of a pressure-control valve to a constant value of $p_{\mathrm{sup}} = 7\,\mathrm{bar}$. The pressure mean value (35) is approximated by

$$\bar{p}(kT_{\mathrm{pwm}}) \approx \frac{1}{N_{\mathrm{pwm}}} \sum_{l=(k-1)N_{\mathrm{pwm}}}^{kN_{\mathrm{pwm}}-1} p(lT_s), \tag{46}$$

with $N_{\mathrm{pwm}} = T_{\mathrm{pwm}}/T_s$. The integral part (41) is realized by the Euler-method, see, e.g., [15].

Experimental results of the trajectory optimization for soft landing were presented in [8]. They show that it is possible to open and close the valve in minimal time with almost zero velocity at the end stops, see [8]. These optimized trajectories are used as feedforward control within the presented pneumatic pulse-width modulation.

A. Parameter Identification

Some parameters of the controller design model (36) are unknown, which is why the nonlinear dynamic least-squares identification task

$$\begin{aligned} \min_{\boldsymbol{\theta}} \quad & J(\boldsymbol{\theta}) = \frac{1}{T_m} \int_0^{T_m} \big(\bar{p}(t;\boldsymbol{\theta}) - \bar{p}_m\big)^2 \mathrm{d}t \\ \text{s.t.} \quad & \frac{\mathrm{d}}{\mathrm{d}t}\bar{p} = \boldsymbol{f}_{\bar{p}}\big(\bar{p}(t;\boldsymbol{\theta})\big), \quad \bar{p}(0) = \bar{p}_0, \\ & \boldsymbol{\theta} = \begin{bmatrix} \Pi_c & C_{\max} \end{bmatrix}^{\mathsf{T}} \geq 0, \end{aligned} \tag{47}$$

with $\boldsymbol{f}_{\bar{p}}\big(\bar{p}(t;\boldsymbol{\theta})\big)$ according to (36), is performed for measurements p_m during the time interval $t \in (0, T_m)$. Just with a little abuse of notation the additional argument should explicitly indicate the dependence on the parameter vector $\boldsymbol{\theta}$. The identification procedure was performed in MATLAB by means of the function `fmincon` using the sequential quadratic programming method in combination with the ordinary differential equations solver `ode15s`. Fig. 8 shows identification results for the charging ($\bar{\dot{m}}_{\mathrm{in}} > 0$ and $\bar{\dot{m}}_{\mathrm{out}} = 0$) and discharging ($\bar{\dot{m}}_{\mathrm{in}} = 0$ and $\bar{\dot{m}}_{\mathrm{out}} > 0$) of the chamber. The results show a good agreement between measurements and simulations, which imply that the model approximations are reasonable.

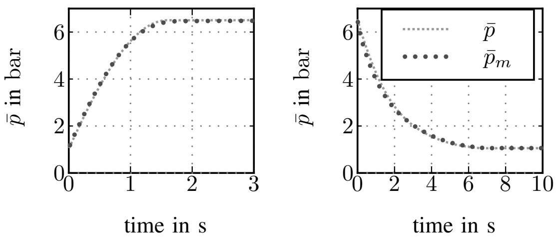

(a) Charging.

(b) Discharging.

Fig. 8: Identification results of the pressure mean model.

B. Measurement Results

Fig. 9 shows measurement results of the pulse-width modulated control strategy for a sinusoidal desired trajectory of the pressure mean value $\bar{p}_d = \bar{p}_a \sin(2\pi f t) + \bar{p}_o$. In Fig. 9a, the parameters are chosen as $\bar{p}_o = 3\,\mathrm{bar}$, $\bar{p}_a = 0.1\,\mathrm{bar}$ and $f = 5\,\mathrm{Hz}$, whereas in Fig. 9b depicts the results for $\bar{p}_o = 5\,\mathrm{bar}$, $\bar{p}_a = 0.1\,\mathrm{bar}$ and $f = 7\,\mathrm{Hz}$. In both cases, a good control performance can be achieved with the presented control strategy.

C. Noise Reduction

To illustrate the noise reduction achieved by the optimized trajectories of the valve, a comparison of the Fast-Fourier transformation of sound recordings from pulse-width modulated pressure control with a simple and with the trajectory optimized valve actuation are depicted in Fig. 10. With the simple switching valve actuation only the maximum voltage to open and the minimum voltage to close is applied to the

Post-print version of the article: T. Glück, W. Kemmetmüller, A. Pfeffer, and A. Kugi, "Pneumatic pulse-width modulated pressure control via trajectory optimized fast-switching electromagnetic valves", in *Proceedings of the 13th Mechatronics Forum, International Conference*, vol. 3/3, Linz, Austria, Sep. 2012, pp. 692–699
The content of this post-print version is identical to the published paper but without the publisher's final layout or copy editing.

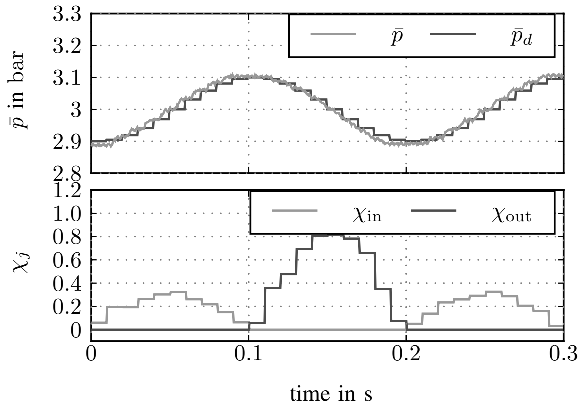

(a) Sinusoidal reference trajectory with $\bar{p}_a = 0.1\,\text{bar}, \bar{p}_o = 3\,\text{bar}, f = 5\,\text{Hz}$.

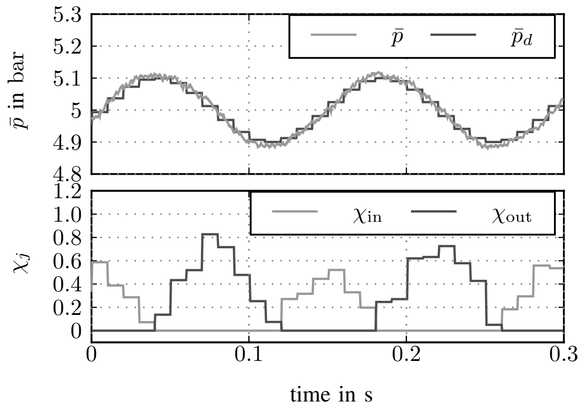

(b) Sinusoidal reference trajectory with $\bar{p}_a = 0.1\,\text{bar}, \bar{p}_o = 5\,\text{bar}, f = 7\,\text{Hz}$.

Fig. 9: Measurement results of the pulse-width modulated pressure control for different sinusoidal desired reference trajectory of the pressure mean value $\bar{p}_d = \bar{p}_a \sin(2\pi f t) + \bar{p}_o$.

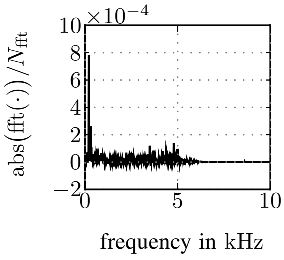

(a) Simple valve actuation.

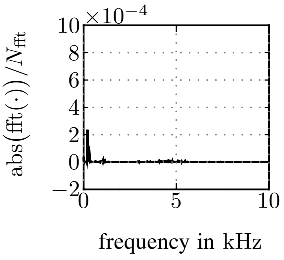

(b) Trajectory optimized valve actuation.

Fig. 10: Fast-Fourier transformation of sound recordings from a simple and from the trajectory optimized valve actuation for a sinusoidal desired trajectory with a frequency of $f = 5\,\text{kHz}$.

valves. The results in Fig. 10 reveal a significant reduction in the frequency range $0 - 6\,\text{Hz}$.

VII. Conclusion

In this work, pulse-width modulated pressure control with fast-switching valves arranged in a half bridge is presented. The fast-switching valves are driven by optimized feedforward trajectories which facilitate soft landing and time optimality. For this, a point-to-point quasi-time-optimal control problem is formulated by means of Pontryagin's maximum principle and numerically solved by a direct approach. The derivation of a mean value chamber model and the identification of its parameters form the starting point for the design of a nonlinear pressure controller. Measurement results on an experimental test bench show the applicability of the proposed pressure control and demonstrate the achievable noise reduction of the pulse-width modulated pressure control in combination with the optimized switching strategy. Future work addresses the extension of the control strategy to pneumatic piston actuators.

Acknowledgment

The authors would like to thank Festo AG [1] for the financial support and cooperation during this joint project.

References

[1] Festo AG, June 2012. www.festo.com.
[2] ISO 6358, June 2012. www.iso.org.
[3] M. Athans and P. Falb. *Optimal control: An introduction to the theory and its applications*. McGraw-Hill, New York, 1966.
[4] A.E. Bryson and Y.C. Ho. *Applied optimal control*. John Wiley & Sons, New York, 1975.
[5] R. R. Chladny and C. R. Koch. Flatness-based tracking of an electromechanical variable valve timing actuator with disturbance observer feedforward compensation. *IEEE Transactions on Control System Technology*, 16(4):652–663, 2008.
[6] S. K. Chung, C. R. Koch, and A. F. Lynch. Flatness-based feedback control of an automotive solenoid valve. *IEEE Transactions on Control System Technology*, 15(2):394–401, 2007.
[7] A.E. Fitzgerald, C. Kingsley, and S.D.Umans. *Electric maschinery*. McGraw-Hill, 6th edition, 2003.
[8] T. Glück, W. Kemmetmüller, and A. Kugi. Trajectory optimization for soft landing of fast-switching electromagnetic valves. In *Proceedings of the 18th IFAC World Congress*, pages 11532–11537, Milano, Italy, Aug. 28 - Sept. 2. 2011.
[9] S. Hodgson, M. Q. Le, M. Tavakoli, and M. T. Pham. Sliding-mode control of nonlinear discrete-input pneumatic actuators. In *Proceedings of the IEEE/RJS International Conference on Intelligent Robots and Systems*, pages 738–743, San Francisco, USA, 22-30 Sept. 2011.
[10] K.A. Hofmann, S.T.L Chiang, M.S. Siddiqui, and M. Papadakis. *Fundamental equations of fluid mechanics*. Engineering Education System, Wichita, 1996.
[11] J. Kierzenka and L.F. Shampine. A bvp solver that controls residual and error. *Journal of Numerical Analysis, Industrial and Applied Mathematics*, 3(1-2):27–41, 2008.
[12] A. Messinaa, N. I. Giannoccaroa, and A. Gentile. Experimenting and modelling the dynamics of pneumatic actuators controlled by the pulse width modulation technique. *Mechatronics*, 15:859–881, 2005.
[13] T. Nguyen, J. Leavitt, F. Jabbari, and J. E. Bobrow. Accurate sliding-mode control of pneumatic systems using low-cost solenoid valves. *IEEE/ASME Transactions on Mechatronics*, 12(2):216–219, 2007.
[14] X. Shen, J. Zhang, E. J. Barth, and M. Goldfarb. Nonlinear model-based control of pulse width modulated pneumatic servo systems. *Journal of Dynamic Systems, Measurement, and Control*, 128:663–669, 2006.
[15] J. Stoer and R. Burlisch. *Introduction to numerical analysis*. Springer, New York, 2002.